RESEARCH ARTICLE

BIOTECHNOLOGY PROGRESS

Cross-scale quality assessment of a mechanistic cation exchange chromatography model

David Saleh[1,2] 🔵 | Gang Wang[1] | Benedict Mueller[1] | Federico Rischawy[1,2] | Simon Kluters[1] | Joey Studts[1] | Jürgen Hubbuch[2]

[1]Late Stage DSP Development, Boehringer Ingelheim Pharma GmbH & Co. KG, Biberach, Germany

[2]Section IV: Biomolecular Separation Engineering, Karlsruhe Institute of Technology (KIT), Institute of Engineering in Life Sciences, Karlsruhe, Germany

Correspondence
Jürgen Hubbuch, Section IV: Biomolecular Separation Engineering, Karlsruhe Institute of Technology (KIT), Institute of Engineering in Life Sciences, Karlsruhe, Germany.
Email: juergen.hubbuch@kit.edu

Abstract

Cation exchange chromatography (CEX) is an essential part of most monoclonal antibody (mAb) purification platforms. Process characterization and root cause investigation of chromatographic unit operations are performed using scale down models (SDM). SDM chromatography columns typically have the identical bed height as the respective manufacturing-scale, but a significantly reduced inner diameter. While SDMs enable process development demanding less material and time, their comparability to manufacturing-scale can be affected by variability in feed composition, mobile phase and resin properties, or dispersion effects depending on the chromatography system at hand. Mechanistic models can help to close gaps between scales and reduce experimental efforts compared to experimental SDM applications. In this study, a multicomponent steric mass-action (SMA) adsorption model was applied to the scale-up of a CEX polishing step. Based on chromatograms and elution pool data ranging from laboratory- to manufacturing-scale, the proposed modeling workflow enabled early identification of differences between scales, for example, system dispersion effects or ionic capacity variability. A multistage model qualification approach was introduced to measure the model quality and to understand the model's limitations across scales. The experimental SDM and the in silico model were qualified against large-scale data using the identical state of the art equivalence testing procedure. The mechanistic chromatography model avoided limitations of the SDM by capturing effects of bed height, loading density, feed composition, and mobile phase properties. The results demonstrate the applicability of mechanistic chromatography models as a possible alternative to conventional SDM approaches.

1 | INTRODUCTION

Over the last decade, ever-rising numbers of monoclonal antibodies (mAbs) in development pipelines increased the demand for novel technologies accelerating mAb process development.[1-3] Multiple publications highlighted the potentialities of in silico process models for rapid and rationalized bioprocess development.[4,5] However, there is so far no consensus within the biopharmaceutical industry on how to apply digital process models to real-world tasks.

Cation exchange chromatography (CEX) is a frequently employed polishing step for the downstream processing (DSP) of mAbs. Its selectivity towards protein charge allows the depletion of high molecular weight species (HMW) and other product and process related impurities.[6,7] HMW removal is of high importance because antibody aggregates may cause an immune response towards the monomeric drug.[8] An in-depth process understanding is crucial for robust process performance and consistent product quality. Development of CEX processes is typically based on a high number of small-scale experiments. Resin selection and process optimization can be performed using automated batch-binding screenings[9,10] and miniaturized column processes.[11-14] Automation, parallelization, and miniaturization are of high value for early stage process development, where a large number of process conditions are screened for numerous mAb candidates. Late stage work packages, such as process characterization, rely on bench-scale experiments using a scale-down model (SDM) column representative for the respective manufacturing-scale unit operation. The SDM, as a physical representation of the manufacturing process, enables effect analysis of process parameters on critical quality attributes (CQA) and key performance indicators (KPI). Hakemeyer et al. described key elements to be considered in SDM design, ranging from impurity levels in load material to the use of sound engineering principles for scaling.[15] In order to keep key process parameters such as residence time and separation distance constant, SDM columns typically have identical bed heights as the respective manufacturing-scale unit operation, but a reduced inner diameter. Furthermore, miniaturized columns for robotic liquid handling stations are currently explored as SDM for chromatographic unit operations.[16] Reduction of column diameter enables a fast and resource-saving development. However, the effectiveness of the purification is not exclusively affected by column dimensions. Variability of input material composition and impurity levels, may impact the comparability between a SDM and its respective large-scale unit operation. Consequently, statistical SDM qualification demands numerous bench-scale experiments with varying input material. Additional effects caused by dispersion in different chromatography systems, resin lot-to-lot variability[17,18] and manual column packing procedures[19,20] may further lead to systematic differences between scales.

In order to follow the quality by design (QbD) concept,[21] biopharmaceutical companies are working on process models to generate an in-depth process understanding.[16,22-25] Mechanistic chromatography models are mathematical representations of the physical effects occurring in the chromatographic system.[26,27] They consist of partial differential equations, describing macroscopic transport through the column, mass transport within the stationary phase, and adsorption of protein to the resin. For mechanistic modeling of mAbs and other proteins in ion exchange chromatography, the SMA adsorption isotherm is frequently used in academic and industrial case studies.[16,28-33] The SMA isotherm describes the multipoint binding of proteins to the resin under consideration of a protein's characteristic charge, the thermodynamic equilibrium of the adsorption process, and steric shielding effects. Multiple studies have demonstrated successful application of mechanistic models for the scale-up of chromatography processes.[14,34,35] Benner et al.[16] used mechanistic modeling to explain systematic offsets between large-scale processes and an experimental SDM based on miniaturized columns for robotic liquid handling stations. The scientific explanation for scaling effects enabled them to utilize the miniaturized system for a parallelized and material saving process characterization study.[16] Ladwig et al.[23] published a mechanistic model describing pH and excipient concentrations for an ultrafiltration and diafiltration (UF/DF) unit operation of a mAb purification process. Similar to the experimental SDM approach, the mechanistic UF/DF model was qualified against large-scale data validating the model's capability to reduce experimental efforts during process development.[23] Beside the capability of explaining scaling effects, the physical principles of mechanistic chromatography models allow the reduction of experimental effort by in silico experimentation at manufacturing-scale.

Successful application of mechanistic models in bioprocess development and manufacturing requires clear guidelines for model development, qualification, and application. As a first building block, we recently introduced a standardized workflow for model calibration to build the quality into the model by applying both, engineering and statistic principles.[36] The subsequent model validation at calibration-scale included 12 experiments with operating conditions beyond the calibration space and the final unit operation. The present study aims to propose the other part of the model quality system with respect to qualifying the mechanistic chromatography model from laboratory- to manufacturing-scale. A multistage evaluation using statistical criteria and engineering knowledge was introduced and applied to measure the quality of model prediction and to understand the model's limitations. Six CQAs and KPIs were derived from the predicted chromatograms and corresponding cutting criteria and compared to the wet-lab purification outcomes. Comparable to the experimental SDM, qualification of the mechanistic model against manufacturing-scale enabled

TABLE 1 Protein specific model parameters for the pH-dependent SMA model

Parameter	APG	Main	BPG	HMW
$k_{eff0,i}$ [mm/s]	1.4E-3	1.4E-3	1.4E-3	1.2E-3
$k_{eff1,i}$ [−]	4.7E-05	4.7E-05	4.7E-05	3.3E-05
$\nu_{pH5.8,i}$ [−]	7.38	7.50	7.70	10.97
$\nu_{1,i}$ [−]	−1.44	−1.44	−1.44	−6.77
$k_{eq,pH\ 5.8,i}$ [−]	1.45	1.41	1.69	1.86
$k_{eq,1,i}$ [−]	−4.26	−4.26	−4.26	−5.39
$k_{eq,2,i}$ [−]	2.19	2.19	2.19	5.59
$k_{kin,i}$ [sM$^{\nu}$]	8.08E-06	1.00E-04	5.00E-04	3.4E-05
σ_i [−]	128.6	56.3	107.1	0

Note: Details regarding the model calibration procedure are described in our previous publication.[36] For a clear representation of model parameters at pH 5.8, the pH was normalized to zero. pH 5.5 = −0.3, pH 5.8 = 0, pH 6.1 = 0.3.

rational evaluation of model predictions for CQAs and KPIs. Direct benchmarking of the mechanistic model against the experimental SDM showed the benefits and perils of both techniques.

2 | MODELING

This section gives an overview on the mechanistic model and complementation necessary for model-guided scale-up. Additional details about model discrimination, model parameters and the model calibration strategy can be found in our previous publication.[36] Protein-specific model parameters were kept constant for all simulations and are listed in Table 1. Simulation and inverse parameter estimation was performed using the ChromX software (GoSilico, Karlsruhe, Germany). Depending on the large-scale chromatography system, pre-column dispersion was approximated by simulating a continuous stirred-tank reactor (CSTR) at the column inlet. Assuming ideal mixing within the CSTR, the change of concentration $c_i(t)$ of component i in Equation (1) is a function of residence time defined by the reactor length L_{CSTR} and superficial velocity u.

$$\frac{\partial c_i(t)}{\partial t} = -\frac{u}{L_{CSTR}}\left(c_{in,i}(t) - c_i(t)\right) \tag{1}$$

The transport dispersive model was selected as column model, due to multiple successful case studies for the simulation of ion exchange chromatography systems.[37-41] Equation (2) describes the macroscopic transport of component i through the chromatography column. The change of the concentration $c_i(x, t)$ is a function of convective mass transport in the interstitial volume, peak broadening caused by axial dispersion D_{ax}, and mass transfer from the interstitial volume into the pore phase of the particle with the radius r_P. Further, mass transfer between the interstitial volume and the particle pores is effected by the interstitial porosity ε_{col} and the effective mass transfer coefficient $k_{eff,i}$. The accumulation of mass in

the pore phase c_i and the stationary phase q_i is described in Equation (3). The Danckwerts' boundary conditions are given in Equations (4) and (5).

$$\frac{\partial c_i(x,t)}{\partial t} = -\frac{u}{\varepsilon_{col}}\frac{\partial c_i(x,t)}{\partial x} + D_{ax}\frac{\partial^2 c_i(x,t)}{\partial x^2} - \frac{(1-\varepsilon_{col})}{\varepsilon_{col}}\left(\frac{3}{r_p}k_{eff,i}\left(c_i(x,t)-c_{p,i}(x,t)\right)\right) \tag{2}$$

$$\frac{\partial c_{p,i}(x,t)}{\partial t} = \frac{3}{r_p}\frac{k_{eff,i}}{\varepsilon_p}\left(c_i(x,t)-c_{p,i}(x,t)\right) - \frac{1-\varepsilon_p}{\varepsilon_p}\frac{\partial q_i(x,t)}{\partial t} \tag{3}$$

$$\frac{\partial c_i}{\partial x}(0,t) = \frac{u(t)}{\varepsilon_{col}D_{ax}}\left(c_i(0,t)-c_{in,i}(t)\right) \tag{4}$$

$$\frac{\partial c_i}{\partial x}(L,t) = 0 \tag{5}$$

Linear flow rates ranged from 155 cm/h to 360 cm/h between investigated scales, demanding the introduction of flow dependencies for the axial dispersion coefficient D_{ax}[42] and effective mass transfer parameter $k_{eff,i}$. The penetration correlation allowed the direct calculation $k_{eff,i}$ for monomer and HMW species at relevant flow rates under consideration of their hydrodynamic radii.[43,44] Within the investigated range, flow dependencies for D_{ax} and $k_{eff,i}$ could be approximated using linear regression, Equation (6) and (7). Experimental validation of D_{ax} and k_{eff} parameters was performed via pulse injections at low loading conditions with dextran and protein, respectively.[36]

$$D_{ax}(u) = D_{ax0} + uD_{ax1} \tag{6}$$

$$k_{eff,i}(u) = k_{eff0,i} + uk_{eff1,i} \tag{7}$$

Protein adsorption is simulated using the semimechanistic SMA adsorption model.[31] The SMA model formulates the equilibrium binding behavior of the protein in consideration of the salt concentration in the pore phase c_s, the ionic capacity of the resin Λ and the proteins characteristic charge ν_i. Equation (8) shows the kinetic form of the SMA isotherm modified by Hahn et al.,[39] where $k_{eq,i} = k_{ads,i}/k_{des,i}$ and $k_{kin,i} = 1/k_{des,i}$ describe adsorption and desorption rates of component i, respectively. In addition, the steric shielding parameter σ_i denotes the number of functional groups on the resin surface blocked by the protein. ν_i and $k_{eq,i}$, the SMA parameters defining the linear region of the adsorption isotherm, were estimated using the Yamamoto method at differing pH values.[45,46] Inverse estimation[37] of the remaining isotherm parameters $k_{kin,i}$ and σ_i was facilitated by designing two experiments representative for the final unit operation. Firstly, a linear gradient elution experiment at 45 g/L loading density contained distinct information on steric shielding and competitive binding effects of the four protein species. Secondly, a step elution experiment at 10 g/L loading density and a counter ion concentration below the set point condition increased the sensitivity for estimating the desorption rate defining $k_{kin,i}$ parameter.

$$k_{kin,i}\frac{\partial q_i}{\partial t} = k_{eq,i}(pH)\left(\Lambda - \sum_{j=1}^{k}\left(v(pH)_j + \sigma_j\right)q_j\right)^{v(pH)_i}c_{p,i} - q_i c_s^{v(pH)_i} \tag{8}$$

$$q_{salt} = \Lambda - \sum_{j=1}^{k} v_j q_j \tag{9}$$

$$k_{eq,i}(pH) = k_{eq0,i} e^{k_{eq1,i}pH + k_{eq2,i}pH^2} \tag{10}$$

$$\nu_i(pH) = \nu_{0,i} + pH\nu_{1,i} \tag{11}$$

The introduction of pH-dependent isotherm parameters is crucial for industrial applications. For the identical mAb polishing step, our previous work showed significant effects on the purification outcome when varying the mobile phase pH between pH 5.5 and pH 6.1.[36] Equations (10) and (11) show the empirical pH dependencies of the characteristic charge ν_i and the equilibrium constant $k_{eq,i}$ developed by Hunt et al.[47] This model was found to be sufficient for the process relevant pH range of pH 5.8 ± 0.3 used in this study.[36]

3 | MATERIAL AND METHODS

3.1 | CEX unit operation

The mAb used in this study is an IgG1 monoclonal antibody expressed in stably transfected Chinese hamster ovary (CHO) cells (Boehringer Ingelheim GmbH & Co. KG, Biberach, Germany). The mAb was captured via Protein A affinity chromatography and further polished using anion exchange chromatography in flow-through mode. The presented mechanistic model describes the subsequent CEX unit operation using the strong CEX resin POROS 50 HS (Thermo Fisher Scientific, Waltham, USA). The process was performed at constant pH 5.8 in bind-elute mode and at a maximal loading density of 45 g/L. The column was equilibrated at a counter-ion concentration of 87 mM Na$^+$, with the same buffer applied to the wash phase after column loading. Subsequently, elution was induced at a counter-ion concentration of 247 mM Na$^+$. For column regeneration and storage, 1 M and 0.1 M NaOH were applied.

Charge variant and HMW concentrations in the elution pool were quantified using analytical CEX chromatography and analytical size exclusion chromatography, respectively. In order to stay consistent with the mass balance for all simulated protein species, the relative percentage of the charge isoforms was calculated based on the monomer concentration obtained from HPSEC analysis. Acidic (APG), neutral (Main) and basic charge variants (BPG), as well as HMW species were considered as CQAs. Process step yield and elution volume were defined as KPIs and quantified using protein concentration determined via absorbance at 280 nm and gravimetric volume measurement. Details about the model calibration strategy and model
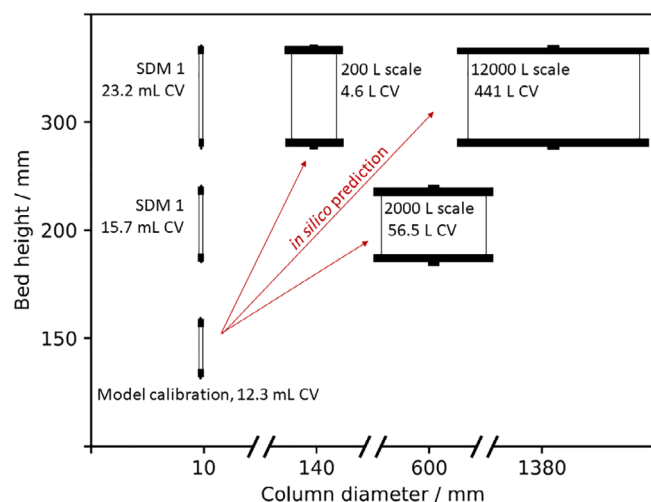

FIGURE 1 Summary of column scales for the CEX unit operation. The mechanistic model was calibrated at bench-scale and applied 200 L, 2000 L and 12,000 L scales. For a clear representation of results, the shown purification scales are named according to the bioreactor volume of preceding cell culture processes. CV, column volume; SDM, scale down model

TABLE 2 System and column specific parameters applied for the simulation of 200 L, 2000 L and 12,000 L scales

Parameter	Symbol	Calibration	200 L	2000 L	12,000 L	Unit
Bed height	L	157	300	200	295	mm
Diameter	d	10	140	6,000	13,800	mm
Column volume	V_{col}	0.0123	4.62	56.6	441	L
Bead radius	r_p	25	25	25	25	μm
Interstitial porosity[a]	ε_{col}	0.41	0.41	0.41	0.41	—
Total porosity[a]	ε_t	0.73	0.73	0.73	0.73	—
Particle porosity[a]	ε_p	0.53	0.53	0.53	0.53	—
Ionic capacity	Λ	0.292	0.310	0.310	0.292	M
Flow rate	u	188	360	240	206	cm/h
Flow rate during elution	$u_{elution}$	188	360	240	155	cm/h
Axial dispersion y-intercept	D_{ax0}	0.0501	0.0501	0.0501	0.0501	mm^2/s
Axial dispersion slope	D_{ax1}	0.2499	0.2499	0.2499	0.2499	mm
CSTR length	L_{CSTR}	—	79	—	—	mm

[a]Porosities were determined at calibration-scale and kept constant across scales.

validation, as well as analytical chromatography methods, are presented in the previous publication of our group.[36]

3.2 | In silico scale-up and model qualification

Figure 1 summarizes scales investigated in this study, ranging from the 12.3 ml column used for model calibration to the 441 L manufacturing-scale column. Additional information about system and column specific properties is listed in Table 2. Model-guided scale-up started with the technical investigation and model development for large-scale chromatography systems. If necessary, system dispersion was simulated by adding a CSTR at column-inlet. Details about system specific effects considered for simulations of each scale are given in section 4.1. For model qualification, the predictive power of the mechanistic model was evaluated across scales. The model was applied to multiple chromatography runs at 200 L, 2000 L and 12,000 L scale. Simulations considered relevant input parameters, such as bed height, flow rate, load material composition, loading density, buffer and resin variability. In the present work, simulations captured the effects of real variances during large-scale experimentation. In contrast, model validation in our previous publication included experiments at challenging operating conditions far beyond the intended set-point condition.[36]

Model qualification consisted of three consecutive stages:

- Investigation of the correlation between predicted and measured CQAs and KPIs across scales: Calculate linear correlation coefficients (R^2) and normalized root-mean-square error of predictions (NRMSEP)
- Testing the statistical significance of the linear correlation: Perform t-test on the slope and intercept of linear regression
- Qualification against manufacturing-scale data using a two one-sided t-tests (TOST)

For scale-independent qualification of the mechanistic model, correlations between predicted and measured values for CQAs and KPIs were evaluated using linear regression and statistical hypothesis testing. t-tests were performed on both, slope and intercept of the linear regression. The tested hypothesis for slope and intercept were one and null, respectively. The NRMSEP given in Equation (11) and (12) was calculated for quantification of the models' predictive power across scales.

$$RMSEP = \sqrt{\frac{\sum_{t=1}^{T}(\hat{y}_t - y_t)^2}{T}} \qquad (11)$$

$$NRMSEP = \frac{RMSEP}{y_{max} - y_{min}} 100\% \qquad (12)$$

In the final step, the predictive capability of the in silico model was compared to the experimental SDM. Following state of the art practices in DSP development, the experimental SDM column had the
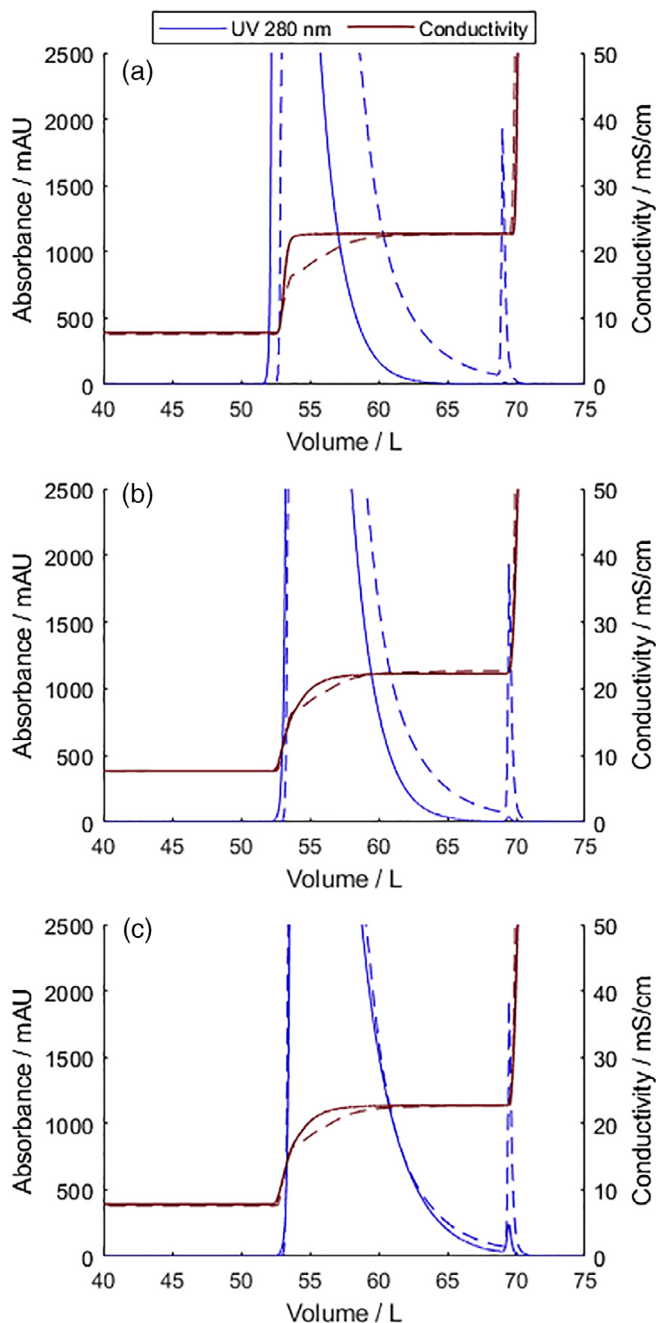

FIGURE 2 Step elution run on the 200 L scale column. Dashed lines show measurement data and solid lines are mechanistic model predictions. (a) Dispersive effects outside the column were neglected during the step elution and ligand density was equal to calibration scale, $\Lambda = 0.292$ M. (b) CSTR in front of the column simulates dispersion caused by the bubble trap, $\Lambda = 0.292$ M. (c) Precolumn CSTR and estimated ligand density, $\Lambda = 0.310$ M

identical bed height as the respective manufacturing process and an inner diameter of 1 cm. To evaluate the comparability between SDM and large-scale, SDM experiments were performed in triplicate with multiple load materials obtained from different large-scale runs. In contrast, mechanistic model simulations considered the variability in the input material, loading density and mobile phase properties for
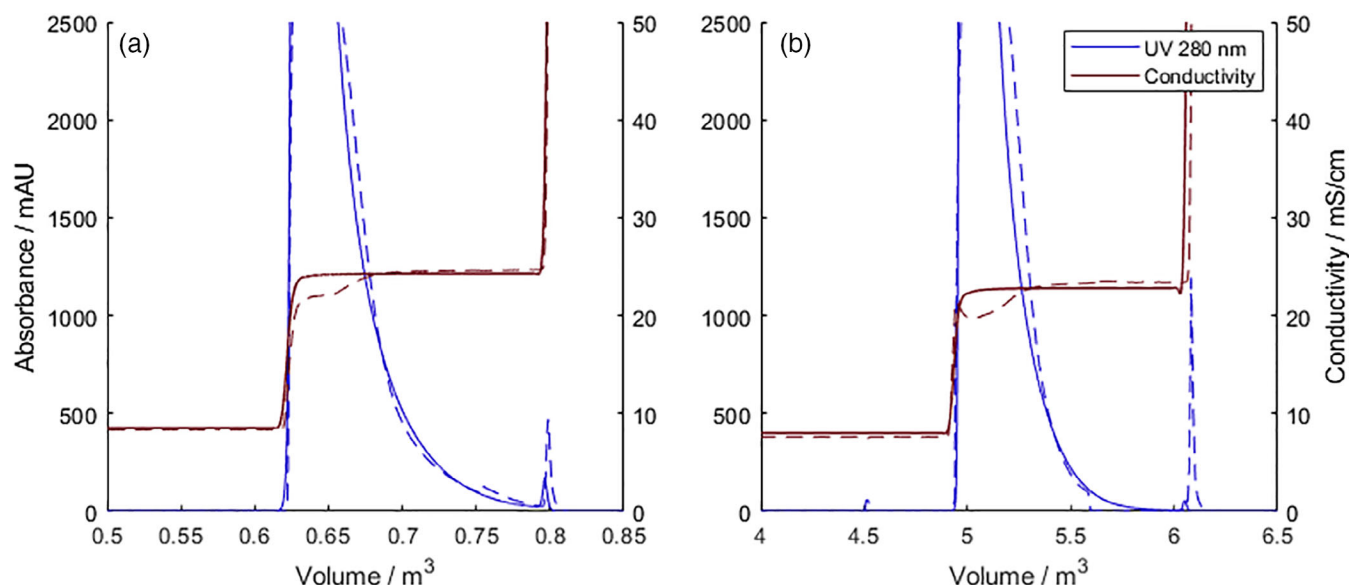
FIGURE 3 Prediction of elution profiles of 2000 L pilot and 12,000 L manufacturing-scale. Dashed lines show measurement data and solid lines are mechanistic model predictions. (a) 2000 L pilot-scale, (b) 12000 L manufacturing-scale

each of the chromatographic cycles. Experimental SDM and mechanistic model were qualified against large-scale data using the identical equivalence testing procedure.[15,23]

- Step 1- Calculation of the equivalence acceptance criteria (EAC) based on the sample mean ± 3 standard deviations (*SD*) of historical large-scale runs.
- Step 2- Equivalence test: A TOST was performed according to Schuirmann[48] using Python 3.8.2. For both, SDM and in silico model, the 90% confidence interval (CI) for the difference in means to large-scale data was compared to the EAC limits. The model was defined as equivalent to the large-scale unit-operation if p-values were below the significance level of $\alpha = .05$.
- Step 3- Visualization and qualification: The 90% CIs of SDM and in silico model difference in means were visualized and compared to the EAC. Model and large-scale unit operation were considered "equivalent", if the 90% CI on the difference in means fell entirely within the EAC. The model was "equivalent in sample mean only", if the 90% CI overlapped with one or both EAC. The model "failed to be equivalent", if the difference in means was located outside the EAC and the 90% CI on overlapped with EAC. When the 90% CI on the difference fell entirely outside the EAC, the model was ranked "not equivalent".[15]

4 | RESULTS AND DISCUSSION

In this work, a mechanistic cation exchange chromatography model calibrated at bench-scale, was applied to chromatography runs of multiple large-scales, including 2000 L pilot and 12,000 L manufacturing-scale. The following chapters describe the approach for the simulation of large-scale systems. Consideration of system dispersion and

variations in ionic capacity between scales enabled the successful qualification of the mechanistic model across scales. For 12,000 L manufacturing-scale, mechanistic model predictions and experimental SDM results were compared considering the most relevant CQAs and KPIs.

4.1 | Simulation of system specific effects

Table 2 shows system and column specific parameters and considerations for simulation of the investigated large-scale chromatography processes. The mechanistic model presented in this study was calibrated at a column bed height of 157 mm. Protein specific mass transfer parameters and SMA adsorption model parameters estimated in our previous publication were applied to simulations of large-scale experiments (Table 1).[36] 200 L, 2000 L, and 12,000 L scale experiments were conducted at differing linear flow rates compared to calibration-scale, demanding the introduction of flow dependent mass transfer parameters. Details about flow dependencies and parameters are given in Section 2, Table 1.

Visual inspection of the conductivity signal at column outlet was the first step of in silico scale-up. This procedure allowed identification and correction of dead volumes and system dispersion effects before simulating protein elution at a new scale. When the salt simulation followed the trend of the conductivity signal, the simulated elution peak was compared to UV measurement data. If further systematic offsets in peak width and retention time were observed, additional evaluation of the elution peak discrepancy was necessary. Variability of resin lot and manual column packing were identified as the most probable root causes for the observed differences between scales causing small variations that were lumped into the ionic capacity. Alternatively, an increased mass transfer resistance resulting in a
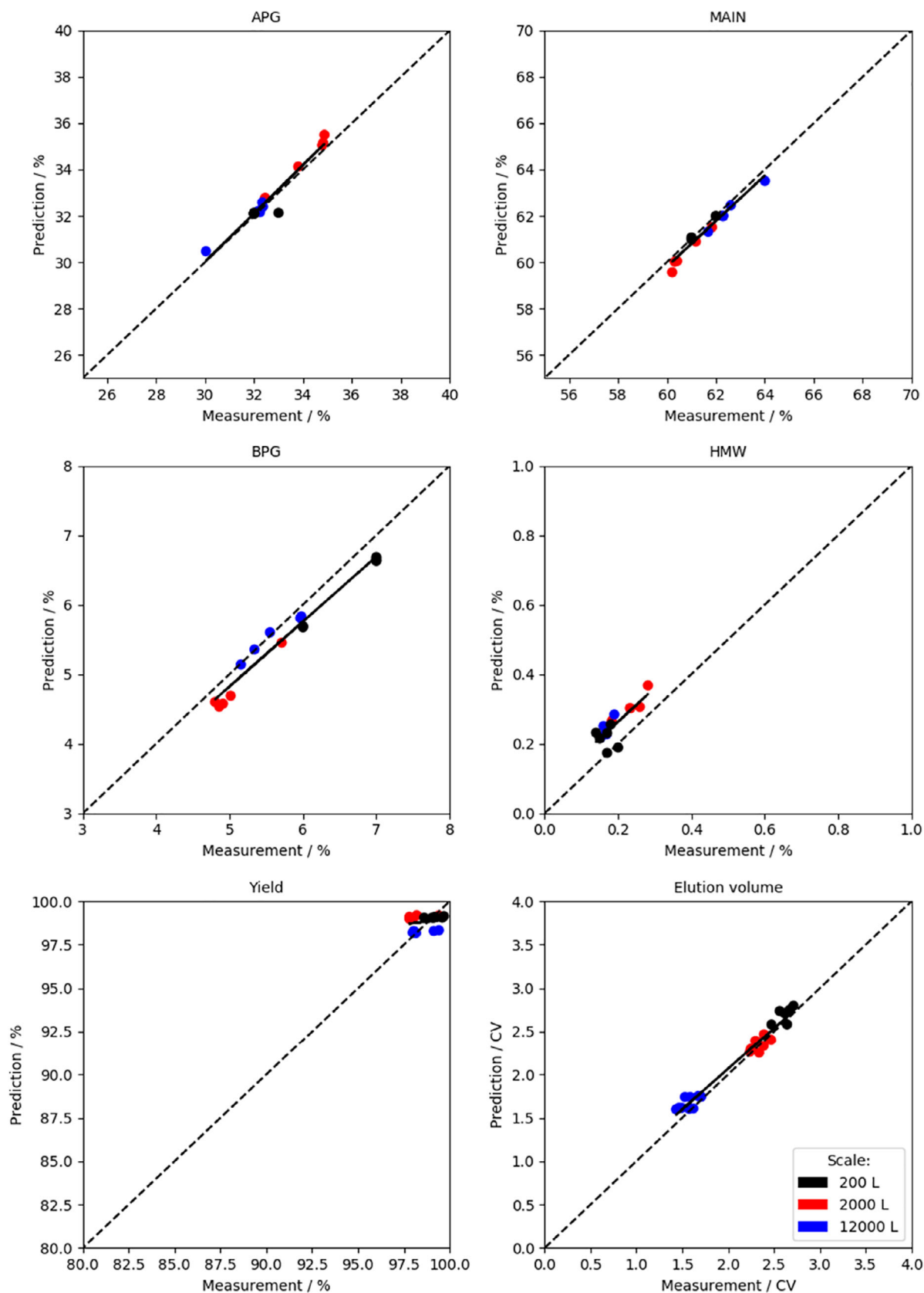
FIGURE 4 Cross-scale analysis of mechanistic model predictions for CQAs and KPI of the CEX unit operation at 200 L, 2000 L and 12,000 L full manufacturing-scale. Solid lines show linear regression for the respective CQA/KPI across scales. CEX, cation exchange chromatography; CQA, critical quality attributes; KPI, key performance indicators

decreased value for k_{eff} could also describe the broadened peak shape. However, a scale-dependent change of k_{eff} is considered less likely compared to variations in ionic capacity, which is a well-known phenomenon in industrial protein chromatography. The direct measurement of ionic capacity using acid–base titration is frequently used for model calibration.[37] However, this potentially harmful procedure is inapplicable to large-scale chromatography columns that are used in compliance with good manufacturing practice (GMP). Further, ionic capacity is normalized to resin backbone volume. Hence, ionic capacity is correlated to column packing density, which complicates the reproduction of acid–base titration of different resin lots in small-scale. Therefore, ionic capacity had to be estimated by applying the inverse method developed by Hahn et al. using a single chromatogram of one scale.[37] The inverse method enabled prediction of all further chromatography runs and all other process outputs at the respective scales. The estimated increase in ionic capacity for 200 L and 2000 L scale was in the range of 6% compared to the calibration-scale. The observed variance in ionic capacity is considered plausible, as the manufacturer specifies the dynamic binding capacity of lysozyme on POROS 50 HS in a range between 57.0 g/L and 75.3 g/L.[49]

Figure 2 depicts simulations of an exemplary 200 L scale chromatogram with and without the final corrections necessary for prediction of conductivity and UV signal. The 200 L scale conductivity signal at column outlet showed a distinctive curvature caused by an increased system dispersion. Compared to other scales, the 200 L scale system was not flushed with high salt buffer before starting step elution. Mixing of wash and elution buffer within the bubble trap led to a comparably slow increase of the conductivity signal. Backmixing within the bubble trap of the 200 L scale system was approximated by simulating a CSTR at the column inlet. As a result, the simulation of the conductivity signal followed the trend of the measured conductivity signal at column-outlet. Further, the slowly increasing salt concentration during step elution and the estimated ligand density corrected retention time and width of the simulated protein peak. System dispersion in 2000 L and 12,000 L scale chromatography systems could be neglected, because the large-scale systems were pre-flushed with elution buffer. The pre-flush led to a steep increase of the conductivity signal and the corresponding salt simulation (Figure 3). Consequently, simulated and measured elution volumes in 2000 L and 12,000 L scale were smaller compared to 200 L scale, shown in Figure 4.

4.2 | Cross-scale qualification of the mechanistic model

This chapter evaluates the predictive power of the mechanistic model across scales. Main differences between scales were column volume, bed height, and flow rate (Table 2). It is important to notice, that all shown chromatography runs were conducted on the set point. Consequently, only small variation in process parameters occurred and their effect on CQAs and KPIs was small compared to the previous model validation at calibration-scale.[36] The small variation of model inputs and outputs further challenged the predictive capabilities and accuracy of the model. Multiple chromatographic cycles were simulated for each scale. Simulations accounted for all variations in load composition, loading density, and mobile phase pH and salt concentrations. In Figure 4, model predictions for CQAs and KPIs of the CEX purification are correlated to the respective measurement data. Investigation of correlation plots are the state of the art procedure in industrial chromatography modeling. However, a decision purely based on these correlation plots is considered too subjective. Hence, linear regression and statistical criteria were introduced for further evaluation of model quality (Table 3).

The very first stage of model qualification is to evaluate R^2 and NRMSEP, since a high R^2 value means the given variances are well covered by the linear regression and a low NRMSEP means the regression line is close to the optimal expectation. In this stage, with $R^2 > .95$ and NRSMEP < 12%, the model's predictive power for the charge variants (APG, Main, and BPG) and the elution volume were confirmed and the qualification is considered as completed successfully. Qualification via R^2 and NRSEMP is considered the case one scenario. Elution volume measurements ranged from 1.4 CV to 2.7 CV. Compared to other CQAs and step yield, the elution volume mainly depended on scale effects, as shown in Figure 4. For simulations of 200 L scale experiments, a pre-column CSTR was added resulting in a larger elution volume compared to other scales. Elution volume of 200 L and 2000 L scale was also increased by a 6% higher ionic capacity compared to 12,000 L manufacturing-scale. Further, the model accounted for the effect of differing bed heights on the elution volume. The 2000 L scale was performed on a column with 200 mm bed height, leading to a higher elution volume compared to 12,000 L scale with 295 mm bed height. It should be noted that model parameters were estimated on a small-scale column with a 157 mm bed height. Also the model validation presented in our previous publication was performed at a bed height of 157 mm.[36] Thus, the

	R^2	NRMSEP [%]	Slope	Intercept	$p_{s,1}$	$p_{i,0}$
APG	.95	7%	1.04	−1.21	.54	.58
Main	.95	8%	0.98	0.86	.77	.81
BPG	.97	12%	0.93	0.15	.15	.56
HMW	.65	49%	0.97	0.07	.89	.09
Yield	.05	37%	0.13	86.12	.00	.00
Elution volume	.97	8%	0.94	0.19	.07	.01

TABLE 3 Regression and *t*-test results for cross-scale model qualification
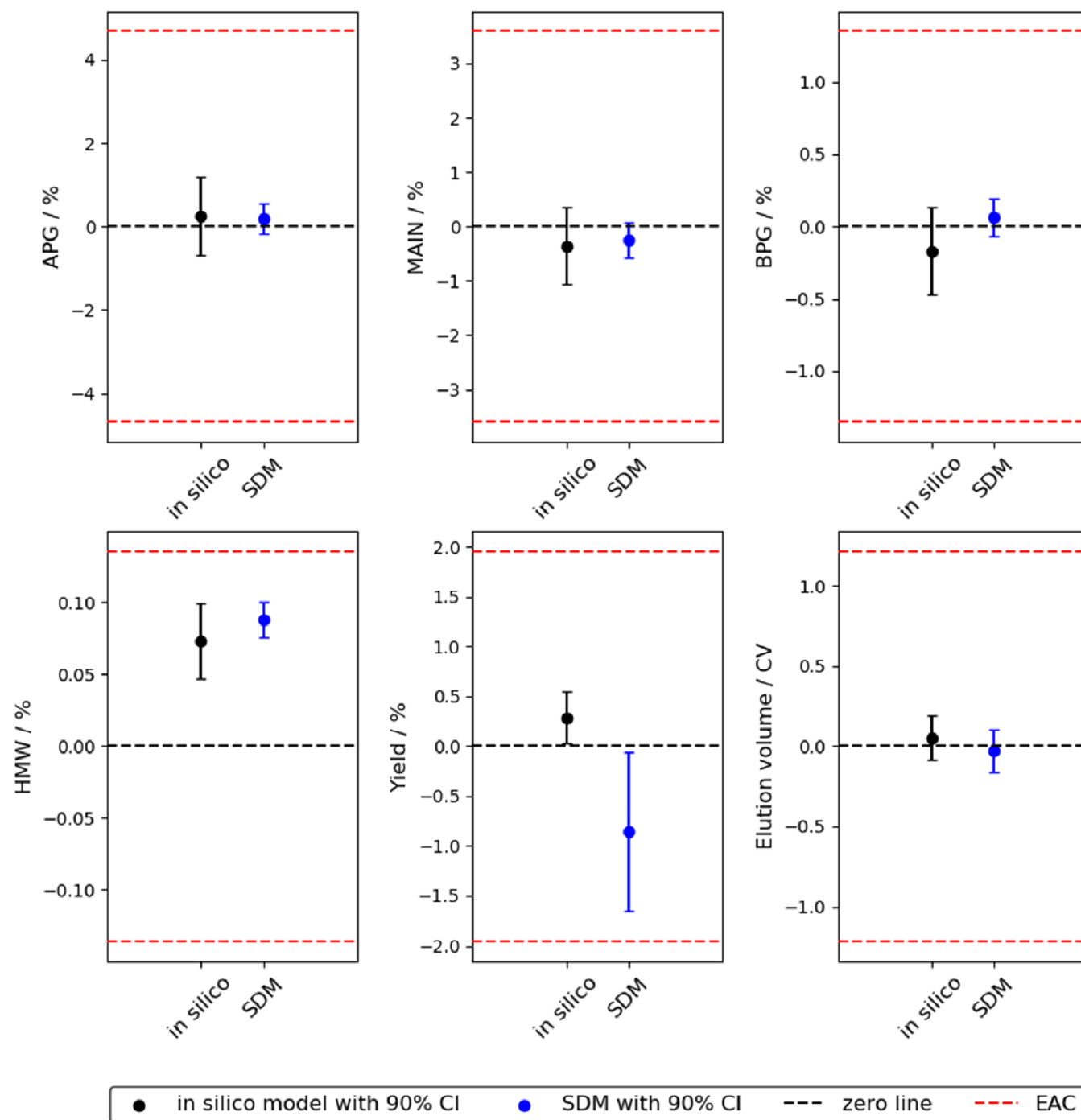
FIGURE 5 Equivalence test comparing large-scale results to mechanistic model prediction and experimental SDM data. Visual representation of TOST analysis. The zero line represents the mean of 20 chromatography cycles for clinical manufacturing. *p*-values were < .05 for all shown CQAs and KPIs. EAC were defined as large-scale mean ± 3*SD* of the respective CQA or KPI. CQA, critical quality attributes; KPI, key performance indicators; EAC, equivalence acceptance criteria; SDM, scale down model

prediction of large-scale runs with increased bed heights further confirmed the plausibility of the estimated model parameters.

For HMW species with both mediocre R^2 = .65 and the NRMSEP = 49%, a second case scenario is described. The distribution of data around the regression line is explained by the very low HMW level in the input material of approximately 0.4% and the elution pool

ranging from 0.14% to 0.28%. Furthermore, total errors of 0.07% in HMW concentrations can originate from analytical method variability and/or different sample handling schemes between scales. In the second scenario, the slope and intercept of the regression line were taken into account being both close to the expectation of being 1 and 0, respectively. The results of a *t*-test with an error-probability of 5%
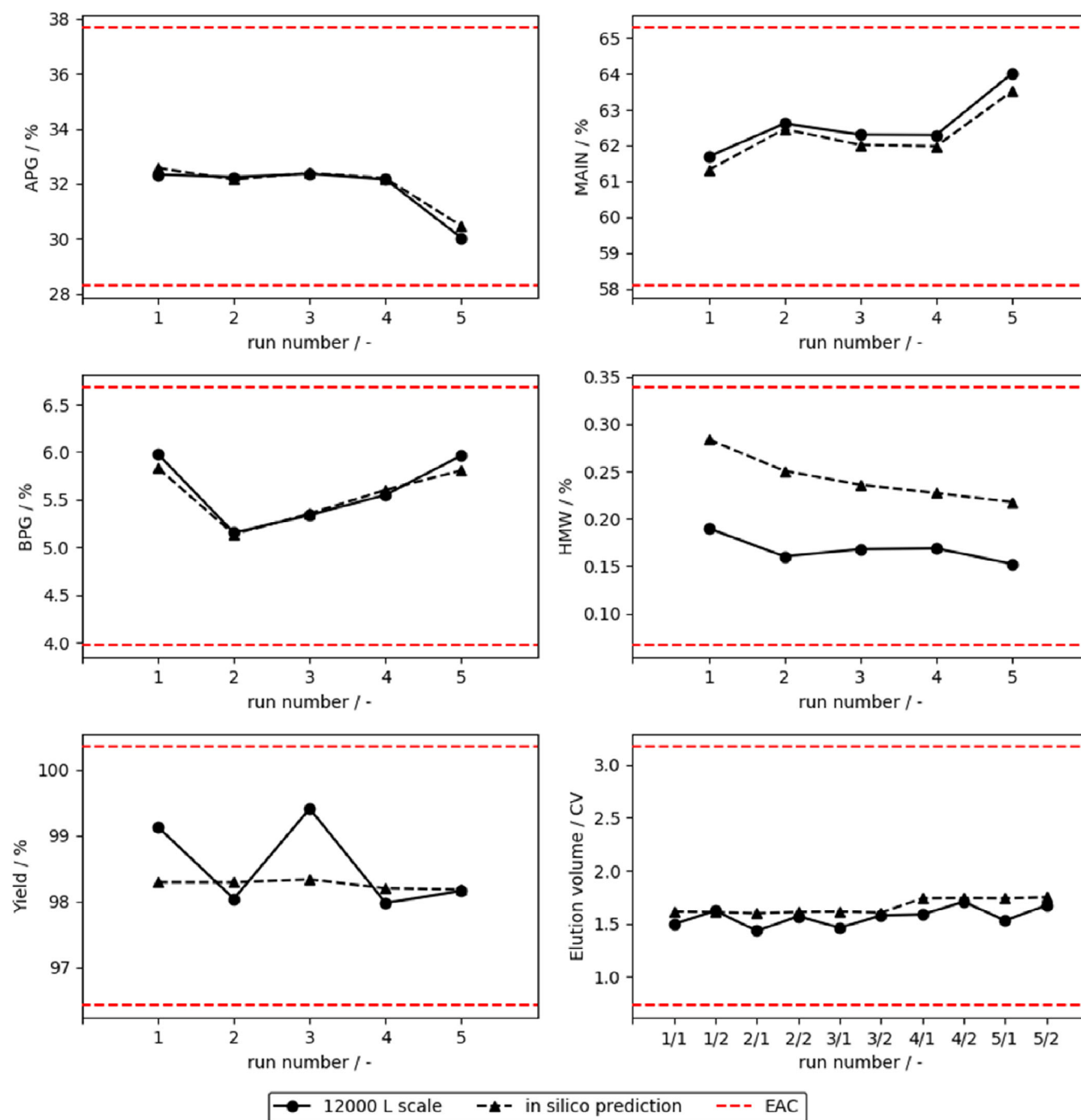
FIGURE 6 Control charts for CQAs and KPIs of 12,000 L scale CEX purification runs. Load composition and mobile phase properties of each simulation were adapted according to the inputs of the respective chromatography cycle. CEX, cation exchange chromatography; CQA, critical quality attributes; KPI, key performance indicators

confirmed the slope and intercept being not significantly different from the expectation. The trust in the model prediction is strengthened by these results from second stage model qualification. Additionally, a systematic shift of HMW concentrations along the y-axis in Figure 4d indicates that the mechanistic model overestimated HMW concentrations for all investigated scales. This over estimation is most likely caused by differences in material and sample handling between manufacturing and process development laboratories. Specifically, the

impact of freeze and thaw on mAb aggregate formation is a well know phenomenon and is the most probable root cause for the observed model offset in the <0.1% range.

The process step yield is considered a third case scenario as neither R^2 and NRMSEP, nor slope and intercept of linear regression support a belief in model prediction. The t-test for slope and intercept of the regression ($p < .05$) rejects the hypothesis, that correlations in slope and intercept are significant. Measured yields across

scales ranged from 97.8% to 99.7%. The observed variance is located within method variability of protein concentration and gravimetric volume measurements of the elution pools. For the investigated experiments, process parameters most likely had no measurable effect on the step yield. Therefore, the model's predictive power of yield is seemingly low and required a direct comparison between the model prediction and the manufacturing-scale outcomes in the final stage of model qualification as presented in the subsequent section.

4.3 | Comparison of mechanistic model with experimental SDM

Equivalence between a process model and its respective full-scale unit operation is the fundamental requirement for applying the model to process characterization studies in late stage DSP development. The TOST is currently the state of the art equivalence testing approach for SDM qualification.[15,23] In Figure 5, the in silico model was qualified against manufacturing-scale data using the TOST qualification scheme described in section 3.2. SDM qualification results are presented as a benchmark for mechanistic model performance. The data included 10 clinical manufacturing runs with two CEX cycles per harvest. The SDM was limited to six load materials of clinical manufacturing runs, with three lab-scale experiments per load material. Further, SDM experiments were conducted with all process parameters at set point conditions. In contrast, the mechanistic model can be seen as a digital twin of the manufacturing-scale process, considering variations in feed composition, column length, as well as mobile phase pH and salt concentration.

The visualization of TOST analysis in Figure 5 qualifies in silico model and experimental SDM for all investigated CQAs and KPIs. The 90% CIs of model predictions were located within the acceptance criteria. Therefore, in silico model and experimental SDM were equivalent to the large-scale unit operation. SDM results and mechanistic model predictions for APG, MAIN, BPG concentrations and elution volume were located close to the mean value of large-scale runs. In contrast, both models consistently overestimated HMW concentrations. The overestimation of HMW concentration was most likely caused by differing sample handling schemes as discussed in the previous chapter. Comparable sample handling procedures for SDM and model calibration experiments in small-scale resulted in similar HMW values for SDM and mechanistic model predictions. In silico predictions for CQAs led to broader CIs compared to the experimental SDM. This observation was caused by the consideration of load material composition in all simulations, while the experimental SDM was limited to six load materials. For example, the percentage of APG species in clinical manufacturing load materials varied between 30.4% and 35.5%, while the SDM only included load materials with 32.1% to 34.1% APG content. The SDM sample mean of yield was located within the EAC, but the error bars indicate a higher variance compared to in silico prediction. This variance was caused by analytical variability of protein concentration and gravimetric volume measurements of the elution pool during SDM experimentation.

The TOST equivalence test is an objective method for model qualification. However, it is difficult to evaluate the true predictive capabilities of the mechanistic model by comparing mean values. Therefore, control charts in Figure 6 compare measured and predicted results of five 12,000 L manufacturing runs with two CEX cycles per harvest. Input data from batch records was used for modeling every chromatographic cycle. Consideration of these input parameters allowed the mechanistic model to predict the trend of CQAs as a function of the run number. Additionally, the mechanistic model enabled quantitative predictions for yield and elution volume within the EAC.

The data shown in this section qualifies the mechanistic model as an in silico representation of the 12,000 L scale unit operation for charge variants, HMW species, step yield and elution volume. Thus, the mechanistic model could be applied to process characterization studies for late stage DSP development. Further, the mechanistic model avoided limitations of the experimental SDM by capturing the minimal effect of process parameter variation on the purification outcome. With a loading density of 45 g/L and a column bed height of 300 mm, a single SDM experiment consumed more protein than the entire model calibration process on the 157 mm column. It is important to notice, that the presented model is limited to the six CQAs and KPIs. Additional CQAs, such as fragments, host cell protein or leached Protein A concentrations need to be added to the in silico model of the CEX unit operation if required.

5 | CONCLUSION

In the presented case study, a mechanistic model calibrated at bench-scale enabled the prediction of chromatography runs in multiple larger scales. In silico experimentation increased process understanding and allowed explanation of offsets between investigated scales. Consideration of scale dependent effects, such as precolumn dispersion and varying ionic capacities was found to be essential for accurate prediction of large-scale CEX processes. All investigated large-scale runs were performed at set-point conditions with only minimal variance of input parameters. The relatively small effect of loading density, input material composition, and mobile phase pH and salt concentration variability on the purification outcome challenged model accuracy. Nonetheless, the consideration of these relatively small input variations together with scale-specific features allowed accurate predictions of CQAs and KPIs across all scales from laboratory to manufacturing-scale. The predictive power across different column dimensions confirmed the physical relevance of the previously estimated model parameters.[36]

For manufacturing-scale, model performance was directly benchmarked against the experimental SDM. The main purpose of qualifying an experimental SDM is to use it in subsequent process characterization studies. Both, SDM and mechanistic model were successfully qualified against manufacturing-scale using well-established equivalence testing procedures. Additionally, the mechanistic model could describe the run-to-run trend of CQAs and KPIs. Therefore, the

application of a thoroughly calibrated and validated mechanistic model for process characterization purposes can be considered as a scientifically sound and suitable complementation to experimental approaches.

This work presents a systematic framework for qualification of mechanistic chromatography models prior to their applications to late stage biopharmaceutical process development. Rules provided allow a more objective and gradual decision-making. However, the definition of model quality criteria is a complex task involving deep technical understanding, statistics, and understanding of the pharmaceutical quality system.

ACKNOWLEDGMENT

ORCID

David Saleh https://orcid.org/0000-0002-1212-3679

REFERENCES

1. Kaplon H, Reichert JM. Antibodies to watch in 2019. *MAbs*. 2019;11 (2):219-238.
2. Kaplon H, Muralidharan M, Schneider Z, Reichert JM. Antibodies to watch in 2020. *MAbs*. 2020;12(1):1703531.
3. Kelley B. Developing therapeutic monoclonal antibodies at pandemic pace. *Nat Biotechnol*. 2020;38(5):1-6.
4. Narayanan H, Luna MF, von Stosch M, et al. Bioprocessing in the digital age: the role of process models. *Biotechnol J*. 2020;15(1):1900172.
5. Baumann P, Hubbuch J. Downstream process development strategies for effective bioprocesses: trends, progress, and combinatorial approaches. *Eng Life Sci*. 2016;17(11):1142-1158.
6. Liu HF, McCooey B, Duarte T, et al. Exploration of overloaded cation exchange chromatography for monoclonal antibody purification. *J Chromatogr A*. 2011;1218(39):6943-6952.
7. Liu HF, Ma J, Winter C, Bayer R. Recovery and purification process development for monoclonal antibody production. *MAbs*. 2010;2(5): 480-499.
8. Rosenberg AS. Effects of protein aggregates: an immunologic perspective. *AAPS J*. 2006;8(3):E501-E507.
9. Coffman JL, Kramarczyk JF, Kelley BD. High-throughput screening of chromatographic separations: I. method development and column modeling. *Biotechnol Bioeng*. 2008;100(4):605-618.
10. Kelley BD, Switzer M, Bastek P, et al. High-throughput screening of chromatographic separations: IV. Ion-exchange. *Biotechnol Bioeng*. 2008;100(5):950-963.
11. Osberghaus A, Drechsel K, Hansen S, et al. Model-integrated process development demonstrated on the optimization of a robotic cation exchange step. *Chem Eng Sci*. 2012;76:129-139.
12. Wiendahl M, Schulze Wierling P, Nielsen J, et al. High throughput screening for the design and optimization of chromatographic processes – miniaturization, automation and parallelization of breakthrough and elution studies. *Chem Eng Technol*. 2008;31(6):893-903.
13. Lacki KM. High-throughput process development of chromatography steps: advantages and limitations of different formats used. *Biotechnol J*. 2012;7(10):1192-1202.
14. Keller WR, Evans ST, Ferreira G, Robbins D, Cramer SM. Use of Mini-Columns for linear isotherm parameter estimation and prediction of benchtop column performance. *J Chromatogr A*. 2015;1418:94-102.
15. Hakemeyer C, McKnight N, John RS, et al. Process characterization and design space definition. *Biologicals*. 2016;44(5):306-318.
16. Benner SW, Welsh JP, Rauscher MA, Pollard JM. Prediction of lab and manufacturing scale chromatography performance using mini-columns and mechanistic modeling. *J Chromatogr A*. 2019;1593: 54-62.
17. Fogle J, Persson J. Effects of resin ligand density on yield and impurity clearance in preparative cation exchange chromatography. II. Process characterization. *J Chromatogr A*. 2012;1225:70-78.
18. Hardin AM, Harinarayan C, Malmquist G, Axén A, van Reis R. Ion exchange chromatography of monoclonal antibodies: effect of resin ligand density on dynamic binding capacity. *J Chromatogr A*. 2009; 1216(20):4366-4371.
19. Keener RN, Maneval JE, Fernandez EJ. Toward a robust model of packing and scale-up for chromatographic beds. 1. Mechanical compression. *Biotechnol Prog*. 2004;20(4):1146-1158.
20. Keener RN, Maneval JE, Fernandez EJ. Toward a robust model of packing and scale-up for chromatographic beds. 2. Flow packing. *Biotechnol Prog*. 2004;20(4):1159-1168.
21. International Conference on Harmonisation of Technical Requirements for Registration of Pharmaceuticals for Human Use, ICH-Endorsed Guide for ICHQ8/Q9/Q10 Implementation. http://www.ich.org/products/guidelines/quality/article/quality-guidelines.html. http://www.ich.org/products/guidelines/quality/article/quality-guidelines.html
22. Mollerup JM, Hansen TB, Kidal S, Staby A. Quality by design— thermodynamic modelling of chromatographic separation of proteins. *J Chromatogr A*. 2008;1177(2):200-206.
23. Ladwig JE, Zhu X, Rolandi P, Hart R, Robinson J, Rydholm A. Mechanistic model of pH and excipient concentration during ultrafiltration and Diafiltration processes of therapeutic antibodies. *Biotechnol Prog*. 2020;(e2993).
24. Shekhawat LK, Manvar AP, Rathore AS. Enablers for QbD implementation: mechanistic modeling for ion-exchange membrane chromatography. *J Membr Sci*. 2016;500:86-98.
25. Shekhawat LK, Pathak M, Sakar J, Rathore AS. Process development in the quality by design paradigm: modeling of protein a chromatography resin fouling. *J Chromatogr A*. 2018;1570:56-66.
26. Mollerup JM. The thermodynamic principles of ligand binding in chromatography and biology. *J Biotechnol*. 2007;132(2):187-195.
27. Nicoud R-M. *Chromatographic Processes*. Cambridge, United Kingdom: Cambridge University Press; 2015.
28. Kluters S, Wittkopp F, Johnck M, Frech C. Application of linear pH gradients for the modeling of ion exchange chromatography: separation of monoclonal antibody monomer from aggregates. *J Sep Sci*. 2016;39(4):663-675.
29. Baumann P, Huuk T, Hahn T, Osberghaus A, Hubbuch J. Deconvolution of high-throughput multicomponent isotherms using multivariate data analysis of protein spectra. *Eng Life Sci*. 2016;16(2): 194-201.
30. Osberghaus A, Hepbildikler S, Nath S, Haindl M, von Lieres E, Hubbuch J. Determination of parameters for the steric mass action model—a comparison between two approaches. *J Chromatogr A*. 2012;1233:54-65.
31. Brooks CA, Cramer SM. Steric mass-action ion exchange: displacement profiles and induced salt gradients. *AIChE J*. 1992;38(12):1969-1978.
32. Briskot T, Stückler F, Wittkopp F, et al. Prediction uncertainty assessment of chromatography models using Bayesian inference. *J Chromatogr A*. 2019;1587:101-110.
33. Rischawy F, Saleh D, Hahn T, Oelmeier S, Spitz J, Kluters S. Good modeling practice for industrial chromatography: mechanistic modeling of ion exchange chromatography of a bispecific antibody. *Comput Chem Eng*. 2019, 106532-undefined;130:106532.
34. Kołodziej M, Sauer DG, Beck J, et al. Scale up of a chromatographic capture step for a clarified bacterial homogenate–influence of mass

transport limitation and competitive adsorption of impurities. *J Chromatogr A*. 2020;1618:460856.

35. Mollerup JM, Hansen TB, Kidal S, Sejergaard L, Staby A. Development, modelling, optimisation and scale-up of chromatographic purification of a therapeutic protein. *Fluid Phase Equilibria*. 2007;261(1):133-139.

36. Saleh D, Wang G, Müller B, et al. Straightforward method for calibration of mechanistic cation exchange chromatography models for industrial applications. *Biotechnol Prog*. 2020;36(4):e2984.

37. Hahn T, Huuk T, Osberghaus A, et al. Calibration-free inverse modeling of ion-exchange chromatography in industrial antibody purification. *Eng Life Sci*. 2016;16(2):107-113.

38. Hahn T, Huuk T, Heuveline V, Hubbuch J. Simulating and optimizing preparative protein chromatography with ChromX. *J Chem Educ*. 2015;92(9):1497-1502.

39. Hahn T, Baumann P, Huuk T, Heuveline V, Hubbuch J. UV absorption-based inverse modeling of protein chromatography. *Eng Life Sci*. 2016;16(2):99-106.

40. Wang G, Briskot T, Hahn T, Baumann P, Hubbuch J. Estimation of adsorption isotherm and mass transfer parameters in protein chromatography using artificial neural networks. *J Chromatogr A*. 2017;1487: 211-217.

41. Borg N, Brodsky Y, Moscariello J, et al. Modeling and robust pooling design of a preparative cation-exchange chromatography step for purification of monoclonal antibody monomer from aggregates. *J Chromatogr A*. 2014;1359:170-181.

42. Chung S, Wen CY. Longitudinal dispersion of liquid flowing through fixed and fluidized beds. *AIChE J*. 1968;14(6):857-866.

43. Bird RB, Stewart WE, Lightfoot EN. *Transport Phenomena*. New Jersey: John Wiley & Sons; 2007.

44. Guiochon G, Felinger A, Shirazi DG. *Fundamentals of Preparative and Nonlinear Chromatography*. San Diego, CA, USA: Academic Press; 2006.

45. Rüdt M, Gillet F, Heege S, Hitzler J, Kalbfuss B, Guélat B. Combined Yamamoto approach for simultaneous estimation of adsorption isotherm and kinetic parameters in ion-exchange chromatography. *J Chromatogr A*. 2015;1413:68-76.

46. Yamamoto S, Nakanishi K, Matsuno R, Kamikubo T. Ion exchange chromatography of proteins—prediction of elution curves and operating conditions. I. Theoretical considerations. *Biotechnol Bioeng*. 1983; 25(6):1465-1483.

47. Hunt S, Larsen T, Todd RJ. Modeling preparative cation exchange chromatography of monoclonal antibodies. In: Staby A, Ahuja S, eds. *Preparative Chromatography for Separation of Proteins*. Somerset, NJ: John Wiley & Sons, Incorporated; 2017.

48. Schuirmann DJ. A comparison of the two one-sided tests procedure and the power approach for assessing the equivalence of average bioavailability. *J Pharmacokinet Biopharm*. 1987;15(6):657-680.

49. Thermo Fisher Scientific Product information sheet: POROS™ strong cation exchange resins: XS and 50 HS; 2018.